DEPARTMENT OF HEALTH AND HUMAN SERVICES

Public Health Service
Centers for Disease Control
and Prevention (CDC)

Memorandum

Date: December 12, 2001

From: Michael J. Galvin, Jr., Ph.D., Lead Program Activity
Office of Extramural Programs, NIOSH, D30

Subject: Final Report Submitted for Entry into NTIS for Grant 1 R03 OH003902-01.

To: William D. Bennett
Data Systems Team, Information Resources Branch, EID, NIOSH, P03/C18

The attached final report has been received from the principal investigator on the subject NIOSH grant. If this document is forwarded to the National Technical Information Service, please let us know when a document number is known so that we can inform anyone who inquires about this final report.

Any publications that are included with this report are highlighted on the list below.

Attachment
cc: Sherri Diana, EID, P03/C13

List of Publications

None to date.

NIOSH Extramural Award Final Report Summary

Title: A Study of Aerosol Transport Using Vortex Methods
Investigator: Michael Flynn, Sc.D.
Affiliation: University of North Carolina
City & State: Chapel Hill, NC
Telephone: (919) 966-3473

Award Number: 1 R03 OH003902-01
Start & End Date: 9/30/1999–9/29/2001
Total Project Cost: $35,164
Program Area: NORA
Key Words:

Abstract:
The long-term goal of this project was to develop a CFD model for assessing respiratory exposure to airborne particulate matter on the basis of aerosol size and density. The discrete vortex method (DVM) was chosen for modeling the airflow in this project because it is well-suited for capturing the time-dependent flow which occurs when a person stands in front of a local exhaust ventilation hood. The original specific aims of this research project were:

1. Write a program which models flow of monodisperse aerosols in the near wake for a bluff body flow, and test the program for solution convergence;

2. Run numerical simulations of air flow and particle motion matching initial conditions of the experiments performed by Helgeson (1992) with mondisperse aerosols having various Stokes numbers flowing past a cylinder, and compare the results of these numerical simulations with data from Helgeson's experiments to identify limitations in the models.

The first specific aim was implemented in a straight-forward manner. Before integrating the DVIVI with the particle-tracking algorithm, benchmark testing of the particle tracking code was performed for a single particle moving in a uniform velocity field. This testing demonstrated good agreement between simulation results and an analytic solution when particle size was at or below 0 (10 1). For larger particle sizes, an error maximum occurred around time 0(ɪ) then vanished over long times. Here, ɪ = particle relaxation time.

During the course of model development, it became obvious that a rigorous test of the convergence properties of the discrete vortex method was required. The DVM was tested at Reynolds numbers of 5,232 and 140,000. For the higher Reynolds number tested here, convergence with respect to the time-averaged characteristics of the flow and validation with experimental data were found easily. Convergence was not demonstrated at the lower Reynolds number.

The second specific aim was not fully accomplished because testing of the airflow model required much effort. Furthermore, it was found that the original dataset to be used was inadequate for validation purposes. For this reason, laboratory experiments were

performed to obtain particle velocities and concentrations downstream of a cylinder. Although polydisperse particles were used in the experiments, the most reliable of these data was for particles with a Stokes number of 0(10-7).

Preliminary testing of the particle-tracking module in conjunction with the DVM revealed sensitivity to particle size and location of particle release into the domain. Furthermore, a more detailed preliminary simulation matching the experimental conditions showed some agreement with the particle concentration field, although this agreement was not in entirety. Comparison of the time-averaged concentration field for this small particle simulation and a tracer gas simulation revealed large differences. The tracer gas had a uniform concentration everywhere in the domain. In contrast, the small particles collected at the edge of the recirculation zone; this high concentration region extends into the far wake of the cylinder. Unfortunately, definitive results were not garnered with the particle tracking code. For this reason, no conclusive statements can be made with respect to the implications of these results for worker exposure to particulate matter.

Publications
None to date.

Final Report: NIOSH R03 OHO3902-01

A Study of Aerosol Transport Using Vortex Methods

Principal Investigator: Michael R. Flynn
Small Grant Investigator: Jennifer Richmond-Bryant

Dept. of Environmental Sciences and Engineering
CB #7400—Rosenau Hall
School of Public Health
University of North Carolina
Chapel Hill, NC 27599-7400

December 30, 2001

Table of Contents

List of Figures

Chapter 1

Abstract

The long-term goal of this project was to develop a CFD model for assessing respiratory exposure to airborne particulate matter on the basis of aerosol size and density. The discrete vortex method (DVM) was chosen for modeling the airflow in this project because it is well-suited for capturing the time-dependent flow which occurs when a person stands in front of a local exhaust ventilation hood. The original specific aims of this research project were:

1) write a program which models flow of monodisperse aerosols in the near wake for a bluff body flow, and test the program for solution convergence;

2) run numerical simulations of air flow and particle motion matching initial conditions of the experiments performed by Helgeson (1992) with mondisperse aerosols having various Stokes numbers flowing past a cylinder, and compare the results of these numerical simulations with data from Helgeson's experiments to identify limitations in the models.

The first specific aim was implemented in a straight-forward manner. Before integrating the DVM with the particle-tracking algorithm, benchmark testing of the particle tracking code was performed for a single particle moving in a uniform velocity field. This testing demonstrated good agreement between simulation results and an analytic solution when particle size was at or below $O(10^1)$. For larger particle sizes, an error maximum occurred around time $O(\tau)$ then vanished over long times. Here, τ = particle relaxation time.

During the course of model development, it became obvious that a rigorous test of the convergence properties of the discrete vortex method was required. The DVM was tested at Reynolds numbers of 5,232 and 140,000. For the higher Reynolds number tested here, convergence with respect to the time-averaged characteristics of the flow and validation with experimental data were found easily. Convergence was not demonstrated at the lower Reynolds number.

The second specific aim was not fully accomplished because testing of the airflow model required much effort. Furthermore, it was found that the original dataset to be used was inadequate for validation purposes. For this reason, laboratory experiments were performed to obtain particle velocities and concentrations downstream of a cylinder. Although polydisperse particles were used in the experiments, the most reliable of these data was for particles with a Stokes number of $O(10^{-7})$.

Preliminary testing of the particle-tracking module in conjunction with the DVM revealed sensitivity to particle size and location of particle release into the domain. Furthermore, a more detailed preliminary simulation matching the experimental conditions showed some agreement with the particle concentration field, although this agreement was not in entirety. Comparison of the time-averaged concentration field for this small particle simulation and a tracer gas simulation revealed large differences. The tracer gas had a uniform concentration everywhere in the domain. In contrast, the small particles collected at the edge of the recirculation zone; this high concentration region extends into the far wake of the cylinder. Unfortunately, definitive results were not garnered with the particle-tracking code. For this reason, no conclusive statements can be made with respect to the implications of these results for worker exposure to particulate matter.

Chapter 2

Significant Findings

The significant contributions of this work are:

1) identifying limitations in the long-time-averaged solution of the discrete vortex method (DVM);

2) collecting an experimental dataset for the near-wake concentration profile of small particles released upstream of a cylinder;

3) developing a particle-tracking module to operate with the DVM; and,

4) acquiring preliminary numerical results illustrating the concentration profile of particles dispersing downstream of a cylinder.

The analysis of a solution for the DVM at Re = 5,232 and Re = 140,000 revealed that the method is better-suited to capturing the long-time-averaged properties of higher-Reynolds number flow than of lower Reynolds number. Specifically, resources were inadequate to prove convergence of the long-time-averaged solution at Re = 5,232, while the Re = 140,000 solution could be verified. Because the lower Reynolds number tested is closer to the flows typically encountered in industrial environments, the implementation of the DVM used in this work is inefficient for capturing human exposure. It is likely that a massively-parallel and/or multipole version of the DVM is needed to demonstrate convergence. Without this standard, no CFD model can be used with any certainty for modeling time-averaged concentrations of airborne substances (gaseous or particulate).

The experimental concentration profile displayed two peak areas. The highest peak was located within the recirculation zone downstream of the cylinder. However, given the low number counts and the low velocities of the air and particles within this region, it is possible that this peak was an artifact of the experimental error analysis technique. Concentration is directly proportional to number count and inversely proportional to particle velocity; hence, low velocities will dominate the concentration. The second peak area was found at the stagnation point located at the end of the recirculation zone. Here, higher number counts were observed. This indicates that particles are actually collecting in this flow convergence zone.

After the particle-tracking module was developed, preliminary runs with small particles released downstream yielded time-averaged particle concentration profiles, which indicate similar collection patterns to those seen in the experiments with a peak at the flow convergence zone. The simulation results show this region to lengthen downstream. However, this simulation did not run until the time-averaged concentration stabilized in all locations in the domain. Other numerical experiments that varied the location of particle injection downstream of the cylinder indicated that the time-averaged concentration of particles within the recirculation zone is highly dependent on the injection site. For the particles released within the recirculation zone, the time-averaged concentration never reached a steady-state level. It is possible that the simulation did not run for a length of time sufficient to see the concentration stabilize. However, it may also be true that there is some violation of mass balance in the nature of the injection within this zone. These preliminary results raise many questions to be explored in future work.

Chapter

3

Usefulness of Findings

The primary goal of this research was to develop a computational fluid dynamics (CFD) methodology for deducing worker exposure to particulate matter. In this vein, the primary benefit of this research lies in the clear presentation of this methodology. Among the specific benefits are: learning about the long-time behavior of vortex methods for capturing the unsteady and time-averaged flow induced by a worker located in front of a local exhaust ventilation hood and producing a particle-tracking code, in conjunction with a vortex method, which allows for analysis of convective and diffusive effects of various-sized particles. Within this study is a clear example of using uncertainty analysis for obtaining more meaningful results from a CFD simulation. Efforts of this nature are needed to set a precedent for the quality of CFD studies to be performed for industrial hygiene applications.

The second benefit of this research was in gaining some insight into the time-averaged breathing zone particulate concentrations arising from these unsteady flows. Results indicate that concentration is dependent upon the initial release point of the particles. When particles are released within the near wake just downstream of the body, it appears that there is a high rate of accumulation within this zone. This behavior was not size-specific. Furthermore, the concentration patterns were analyzed for small particles released far upstream of the body. In this case, breathing zone concentrations appear to be slightly higher than those in the freestream, while higher concentrations are found at the edge of the near wake region. These observations imply that breathing zone concentrations may be much higher when particulate matter is released directly in front of the worker. If confirmed, hygienists might use this information to deduce when simple local exhaust ventilation is sufficient and when additional protective measures, such as personal protective equipment or downdraft ventilation, are needed. However, it is essential to emphasize that all results obtained to date with the particle-tracking module of the code are preliminary in nature. They do not yet constitute a definitive picture of the concentration profile for particles within the breathing zone of a worker.

Chapter 4

Scientific Report

Specific Aims

The overall objective of this research was to develop a computational fluid dynamics model for assessing respiratory exposure to airborne particulate matter on the basis of aerosol size and density. The purpose of this model was for industrial hygienists to use output results for selecting the most appropriate controls for a given exposure.

The original focus of this pilot study was to develop a method to model particle concentration in the worker's breathing zone using a Discrete Vortex Method (DVM) for the airflow. The code was then to be tested for convergence and validated against an experimental data set, according to the following tasks:

1) Write a program which models flow of monodisperse aerosols in the near wake in a bluff body flow, and test the program for solution convergence;

2) run numerical simulations of air flow and particle motion matching initial conditions of the experiments performed by Helgeson (1992) with mondisperse aerosols having various Stokes numbers flowing past a cylinder, and compare the results of these numerical simulations with data from Helgeson's experiments to identify limitations in the models.

Background

The size-dependent health effects of particulate matter are well-known and well-documented (Soderholm, 1989; NIOSH, 1991; Witschi & Last, 1996; Soutar et. al., 1997). Given the far-reaching breadth of the problem of controlling particulate exposure in industry, hygienists constantly seek mechanistic explanations for exposure events. Particle concentration in a worker's breathing zone depends on the air velocity field around that worker (George et. al., 1990; Flynn and George, 1991; Flynn and Miller, 1991; Guffey and Barnea, 1994; Dunnett, 1994; Flynn et. al., 1995; Kulmala et. al., 1996; Andersson et. al., 1997; Brohus, 1997; Saamanen et. al., 1998). If he or she is working in front of a local exhaust ventilation hood, air can be pulled from behind the worker, separate at the sides of the body, and form a recirculating wake in front of the worker. That flow is composed of a mean, periodic, and random component. The periodic component is driven by vortex shedding; this is thought to be the primary mechanism of contaminant transport in and out of the wake (Flynn and Miller, 1991). Hence, capturing time-dependent vortex shedding in an exposure model may be essential to creating a realistic depiction of exposure. Because the DVM is capable of capturing the time-dependent shedding motion, it was chosen to model the airflow. For the reviewer's convenience, the DVM is explicated in detail below, along with a description of the modeling techniques used to obtain the particle concentration field.

Fluid Modeling

The Discrete Vortex Method (DVM), developed by Chorin (1973, 1978) was used to capture the unsteady airflow in this project. The DVM does not assume turbulence induced by smaller scales is significant, unlike k~ε models where energy from smaller scales of turbulence is manifest in μ_t (Chorin, 1973; Launder & Spalding, 1974). Rather, solution of the vorticity-transport form of Navier-Stokes

reveals only the largest-scale eddies present in the flow. The DVM is self-adaptive so that the fluid is discretized by a group of discrete elements that move in time throughout the domain, in contrast to a fluid whose velocity is computed everywhere over a gridded domain. This formulation avoids numerical viscosity, or over-prediction of the viscosity based on errors arising from grid discretization (Chorin, 1973). Furthermore, although smaller eddies are not represented, modeling large-scale eddies is often adequate for capturing the transient phenomenon of periodic vortex shedding.

The governing equations of fluid motion can be written in terms of the vorticity-transport form of the Navier-Stokes equations. The flow is considered to be purely two-dimensional; hence, the cylinder is assumed to be infinitely long. Operator splitting is employed to solve vorticity-transport by dividing it into a convective and diffusive portion.

The vortex method also accounts for boundary layer flow, because flow separation at the sides of the body incites vortex formation in the wake (Schlichting, 1979). At the beginning of the simulation, two side-by-side eddies will separate, one from each side perpendicular to the freestream, and grow immediately downstream of the cylinder. This stable bubble will grow until some small perturbation causes the velocity field to become unstable. The perturbation can be provided by an approximation in Δt or by the random walk, to be described below, in lieu of refinement to convergence followed by a deliberate perturbation as in Anderson et. al. (1990). This instability causes the eddies to separate from the body in an alternating pattern to produce the Kármán vortex street.

Within the thin boundary layer, order of magnitude analysis reveals that the flow is subject to Prandtl's boundary layer equations. Figure 1 displays the global and boundary layer coordinate systems with respect to the cylinder. Elements of fluid will only diffuse in the direction normal to the cylinder (Chorin 1978; 1980). At the cylinder surface, no-flow and no-slip boundary conditions must be enforced. Also note that the boundary layer equations can be split into convective and diffusive portions in the same manner as done for the vorticity-transport equations.

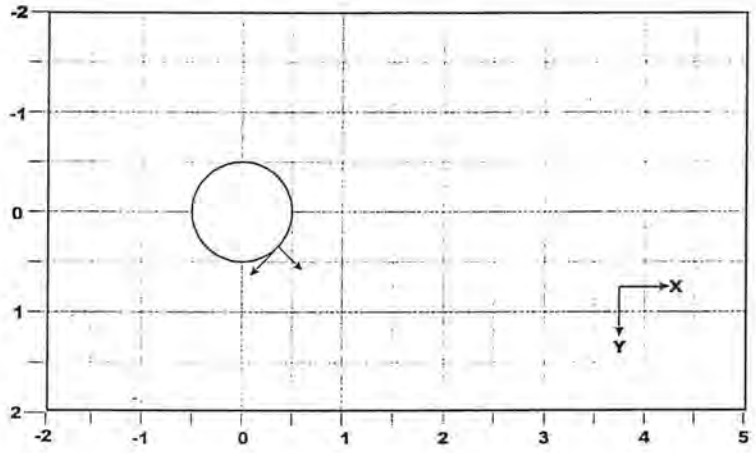

Figure 1. Computational domain used for discrete vortex simulations.

The DVM is implemented through a series of steps. At the beginning of the first time-step, only a freestream velocity exists. The first step in the method and at each subsequent time-step is to generate a cylinder and enforce the boundary condition of no flow through the boundary. This is accomplished with a submerged panel method (Anderson et. al., 1984; Tiemroth, 1986).

The next step is to generate vortex sheets at the surface of the cylinder to enforce the no-slip boundary condition. At each control point, sheets having length $h=\pi D/n_c$, where n_c is the number of control points, are generated with total vortex strength proportional to twice the tangential velocity at the control

point. After the sheets are newly generated, they diffuse through a full time-step. Diffusion is simulated by a random walk having zero mean and variance $\sigma \approx 2\nu\Delta t$. New sheets that diffuse into the cylinder are removed from the simulation. Sheets that diffuse outward will be designated as old sheets, if they remain in the numerical boundary layer having a thickness proportional to $Re^{-1/2}$, or as blobs if they diffuse past the edge of the numerical boundary layer (Chorin, 1978; Cheer, 1983). Blobs are elements of fluid which have circulation equal to the product of sheet length and vortex element strength. To avoid a singularity resulting from infinite vorticity at the center of the blob, a cutoff radius, l, is imposed; this effectively eliminates from the simulation any eddies smaller than the cutoff radius (Chorin, 1973). Use of this formulation for the numerical boundary layer thickness ensures that the size of the boundary layer will be proportional to the viscosity.

In subsequent time-steps, vortex elements are transported according to Euler's equation and diffusion by the method of fractional steps, which is implemented as one-half a diffusion step, a full convection step, and another half diffusion step. Blobs can diffuse in either direction because they are not influenced by the motion of the boundary layer. For both blobs and sheets, one-half the variance is used to calculate the random walk for the half-step (Chorin, 1973). Convection is computed by a first-order finite-difference solution of Euler's equation with the velocity determined according to the Biot-Savart equation. Details elucidating these computations are given in Chorin (1973, 1978) and in Cheer (1983), among others.

At the end of each fractional step, a two-fold process of vortex element metamorphosis takes place. First, the position of each vortex element is checked by the code. If the element lies within the numerical boundary layer, it is designated as a sheet; if the element lies outside the boundary layer, it is designated as a blob. When a sheet is converted to a blob, its sheet strength, γ, is converted to a circulation, $k = \gamma h$. A second procedure is applied when a sheet or blob moves into the cylinder. If the element moves into the image boundary layer, which is located on the interior edge of the cylinder and has the same thickness as the numerical boundary layer, the vortex element is reflected back into the numerical boundary layer according to the law of cosines (Ghoniem, Chorin, & Oppenheim, 1982). If a blob moves past the image boundary layer, it is removed from the computation, while a sheet that moves past the image boundary layer is reflected as a blob. Because the occurrence of sheet and blob removal after contact with the cylinder is very rare, this has a negligible impact on conservation of mass.

At this point, velocity components have been computed, and the code begins a new time-step with the potential flow solver.

Particle Transport Modeling

For particles outside the Stokes regime, the particle equation of motion as given by Michaelides (1997) was integrated using the Backwards Difference Formulae method (BDF). A BDF integrator was chosen because preliminary studies for this project demonstrated that it is more accurate and less computationally-intensive than other integration methods, such as Runge-Kutta methods. In the case where particles are small enough to assume that they follow the airflow exactly, the velocity of the air at the location of the particle is considered to be the particle velocity. For either large or small particles, two half-diffusion routines using the particle's diffusivity coefficient to determine the standard deviation of Brownian diffusion flank the convection routine, as is done for the fluid operator-splitting algorithm.

Computation of Particle Concentration

The primary goal of this project was to estimate the concentration of particles in the worker's breathing zone when the worker is immersed in a time-dependent velocity field created by the local exhaust ventilation hood. Lu et. al. (1992, 1993) devised a method for computing the time-averaged particle number concentration, $\bar{C}$, over a fixed domain when the particle trajectories are computed simultaneously with the fluid motion:

$$\bar{c} = \frac{1}{VN} \int_{d_1}^{d_2} \psi(l) \left[\int_{t_1}^{t_2} \Phi_i^N(t,l) dt \right] dl \qquad (1)$$

where $\Phi_i(t,l)$ = number of particles of a given size interval passing through the domain at a time interval (t_1, t_2)

$\psi(l)$ = particle size distribution function

d_1, d_2 = lower and upper interval bounds on particle size

V = computational domain volume

N = total number of particles passing through the domain during the simulation

l = integration variable for particle size.

Equation (1) is executed for the time-dependent simulation by superimposing a grid over the domain, counting the number of particles in each grid cell, and then factoring that number into a time-averaged particle concentration for each cell.

Implementation

In the course of the project, it became necessary to adjust the tasks originally specified for this project. These adjustments did not change the overall project goal; rather, they were necessary steps that were not obvious at the beginning of this project. Changes to each specific aim are enumerated:

1) Write a program which models flow of monodisperse aerosols in the near wake in a bluff body flow, and test the program for solution convergence.

The architecture of the particle-tracking module of the DVM was similar to the plans originally specified. Additionally, the effect of particle diffusion was included by adding a random walk, based on the particle's coefficient of diffusion, to the position of the particle. For very small particles, the air velocity was used for particle convection in place of the BDF integration of the particle equation of motion because very small particles relax to the air motion within microseconds.

Prior to integrating the particle-tracking algorithm with the DVM, it was first tested independently using the benchmark case of a single particle moving through a uniform flow field. This simple case was investigated because an analytic solution for the velocity of a particle traveling in a uniform flow exists (Michaelides, 1998):

$$V = V_0 + (U - V_0)\{1 - [(1 + 0.15\mathrm{Re}_f^{2/3})e^{2/3\tau} - 0.15\mathrm{Re}_f^{2/3}]^{-3/2}\} \qquad (2)$$

where V = particle velocity, U = fluid velocity, t = time, τ = particle relaxation time, and Re_f = fluid Reynolds number (= $\rho d_p U/\mu$), ρ = fluid density, d_p = particle diameter, and μ = dynamic viscosity. Note that Re_f is based on the length scale of the particle. The particle was tracked along multiples of the relaxation time from an initial velocity or from rest until it relaxed to the velocity of the air stream. Simulation conditions for these tests are listed in Table I. Note that ε is the error tolerance used in the backwards difference formulae integration routine.

Simulation	d_p (μm)	u_{x0} (m/s)	u_{y0} (m/s)	v_{x0} (m/s)	v_{y0} (m/s)	ε	Δt (s)
1	3.4	0	1	0	0	1×10^{-12}	0.01τ, 0.05τ, 0.1τ, 0.5τ, τ
2	3.4	0	1	0	0	5×10^{-16}	0.01τ, 0.05τ, 0.1τ, 0.5τ, τ
3	3.4	0	1	2	2	5×10^{-16}	0.01τ, 0.05τ, 0.1τ, 0.5τ, τ
4	34	0	1	0	0	1×10^{-12}	0.01τ, 0.05τ, 0.1τ, 0.5τ, τ
5	34	0	1	0	0	1×10^{-15}	0.01τ, 0.05τ, 0.1τ, 0.5τ, τ
6	340	0	1	0	0	1×10^{-10}	0.01τ, 0.05τ, 0.1τ, 0.5τ, τ
7	340	0	1	0	0	1×10^{-12}	0.01τ, 0.05τ, 0.1τ, 0.5τ, τ
8	3400	0	1	0	0	1×10^{-5}	0.01τ, 0.05τ, 0.1τ, 0.5τ, τ
9	3400	0	1	0	0	1×10^{-8}	0.01τ, 0.05τ, 0.1τ, 0.5τ, τ

Before enacting full convergence studies of the particle-tracking algorithm, the time-averaged requirement of the particle-tracking code necessitated careful analysis of the DVM's long-time behavior. Verification, or convergence testing, and validation, comparison with experimental results, was performed for Re = 5,232 and Re = 140,000. Verification is carried out following the method used by Sethian and Ghoniem (1988) by refining the time-step and number of vortex elements until coherent eddies appear and vortex shedding frequency and length of the time-averaged recirculation zone downstream of the cylinder, L_B, have stabilized. The lower Reynolds number simulation was validated through comparison with experimental data generated for this work, while the higher Reynolds number solution is compared with experimental data obtained by Cantwell and Coles (1983). These findings are also presented in the next section.

Simulation	*Re*	Δt	k_{max}	N_1
A	5,232	0.0125	0.0005	12,289
B	5,232	0.025	0.002	3,265
C	5,232	0.05	0.008	525
D	140,000	0.0125	0.0005	11,159
E	140,000	0.025	0.002	2,962
F	140,000	0.05	0.008	524
G	140,000	0.075	0.016	444

Table II. Discrete vortex method model input parameters.

Table II lists the input parameters used for simulations A-F. Note that k_{max} is defined as the maximum circulation of a blob, i.e. the product of the maximum vortex element strength and the sheet length, and that N_1 is the number of elements when $t = 1$, chosen arbitrarily to compare the relative magnitude of the number of elements in the domain for each simulation. The number of discretisation panels was always kept at 40 because no significant change in output could be detected when the number of panels was doubled to 80.

2) Run numerical simulations of air flow and particle motion matching initial conditions of the experiments performed by Helgeson (1992) with mondisperse aerosols having various Stokes numbers flowing past a cylinder, and compare the results of these numerical simulations with data from Helgeson's experiments to identify limitations in the models.

Further analysis of Helgeson's (1992) data set revealed that the size of the cylinder used in his experiments was on the order of the size of the laser crossing used to make phase Doppler anemometer (PDA) measurements. This configuration adds too much uncertainty to the location of each measurement to have meaningful results. For this reason, it was necessary to perform laboratory experiments for particle transport past a circular cylinder with a phase Doppler anemometer measurement technique. The acquired data set will serve for validating upcoming particle transport simulations.

Experiments were performed in a recirculating wind tunnel located at the U.S. Environmental Protection Agency's Atmospheric Methods and Monitoring Branch (Research Triangle Park, NC). The tunnel consists of a blower powered by a 50-hp motor and which draws air downstream through a set of louvers. As the air passes the corner opposite to the blower, a set of direction vanes guides the air, which then flows through a turbulence grid with 4" x 4" openings. After passing through a contraction, the air encounters a honeycomb grid, which removes any large-scale turbulent structures from the flow. Finally, the air travels downstream to the 1.52 m x 1.21 m x 7.30 m test section where velocity measurements are taken with a three-dimensional Helium-Neon laser PDA (Dantec Measurement Technology, Inc., Copenhagen, Denmark), which is described in detail in many publications including Durst & Whitelaw (1971), Foreman, George, & Lewis (1965), and Rudd (1969). Tunnel speeds can reach up to 6.67 m/s. For a freestream velocity of 1.0 m/s, the tunnel velocity profile is uniform over the cross-section with a spatial coefficient of variation of 3.0%; the turbulence intensity at this speed is 3.5%. A detailed description of this tunnel can be found in Heist et. al. (2001).

Experiments for validating the Re = 5,232 simulation were performed at a velocity of 1 m/s past a 0.0762 m diameter, 1.17 m tall smooth circular cylinder. The presence of the aluminum cylinder results in 4.8% blockage over the tunnel cross-sectional area. The cylinder is just slightly shorter than the 1.21 m high wind tunnel test section. Figure 2 shows the placement of the cylinder within the test section. Polydisperse solid spherical aluminum silicate particles (Zeeospheres™ W-610, 3M, St. Paul, MN) were released far upstream of the test section and mixed with the air before passing through the honeycomb and entering the test section (Heist et. al., 2001). The experimental data were classified by size, and 3.4 μm particles were used in the final analysis because this size gave the most data at each location. Additionally, to detect the air motion, propylene glycol smoke particles were released into the air by a theatrical smoke generator (Martin Magnum Pro 2000, Århus, Denmark).

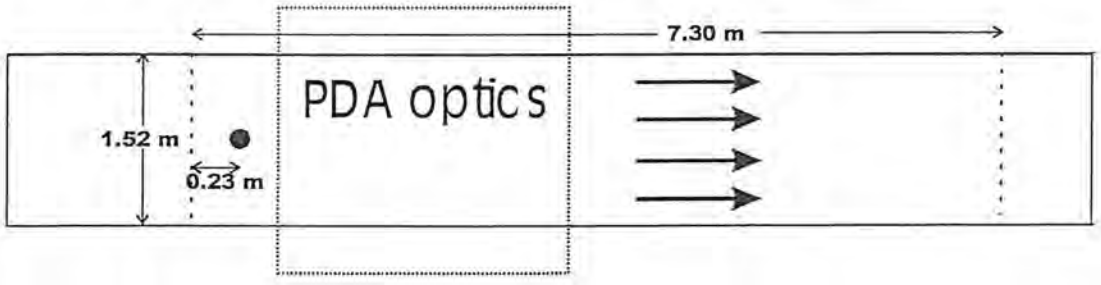

Figure 2. Planview of the wind tunnel test section. ---- denotes beginning and end of the test section.

Particle velocity was measured with the PDA at 102 positions downstream of the cylinder, and air velocity (seeded with smoke) was measured with the PDA at 140 positions downstream. Axi-symmetry allowed for measurement on only one side of the cylinder. Measurements were made at only one height, 0.61 m above the floor and were taken at $0.625 \leq x/D \leq 4$ and $0 \leq y/D \leq 0.75$ with the origin located at the cylinder centre. Measuring points were spaced 0.125 diameters apart to obtain a detailed picture of the recirculation bubble downstream of the cylinder. A beam power of 3 W was maintained to eliminate noise from small particles (Drain, 1972; Lading, 1973), and velocities from particles yielding a signal-to-noise (*S/N*) ratio less than +1 dB were omitted to avoid bias in the velocity calculation (Ibrahim, Werthimer, & Bachalo, 1990).

From the time series of data collected at each measurement point, information about particle and air velocity, particle concentration, and turbulence intensity was calculated. 95% confidence intervals for the velocity were computed based on turbulence intensity and measurement uncertainty resulting from *S/N* and sampling independence. Details of each computation are given in Høst-Madsen (1994) for *S/N* and in George (1979) and in Winter, Graham, & Bremhorst (1991) for sample independence. It was evident from the analysis that uncertainty was dominated (>> 90%) by turbulence intensity for the majority of the data acquired behind the cylinder.

Results and Discussion

Benchmarking the Particle-Tracking Code: Results

Figures 3-11 show the results for the tests with a single particle moving through a uniform flow field for simulations 1-9, respectively.

Timestep size Δt, and error tolerance, ε, used within the BDF solver to control local errors in computing V were adjusted to test the particle-tracking module's ability to converge to a physical solution. Various particle sizes were investigated to ascertain the range of applicability of the code. Experimentation showed that reduction of ε led to smaller truncation errors so that convergence could be obtained primarily through reduction of Δt. For example, when a 3.4 μm particle is released from rest in a uniform freestream velocity of 1 m/s, when $\varepsilon = 1 \times 10^{-2}$, error between numerical results for particle velocity and the analytic velocity obtained from equation (2) is unpredictable with respect to Δt. When error tolerance is reduced further to $\varepsilon = 1 \times 10^{-12}$, a decreasing relationship between Δt and error is evident for all but the smallest Δt tested; this is demonstrated in figure 1, which shows particle velocity versus time for simulations with various Δt and for the analytic solution. For $\varepsilon = 5 \times 10^{-16}$, the error between numerical and analytic solutions has decreased for each Δt; meanwhile, the decreasing relationship between Δt and error is maintained for all except the smallest Δt, as shown in figure 2. Similar behavior is found for 3.4 μm particles having initial velocity of $u_p = 2$ m/s, $v_p = 2$ m/s and moving in the same uniform air stream, as shown in figure 3. However, for larger particles (34-3400 μm), reducing ε below some threshold actually caused the errors to begin to increase with respect to the analytical solution. Despite this, error still decreased with respect to decreasing Δt. Here, trends in the relationship between Δt and error are similar to that seen in figure 2 for all cases presented.

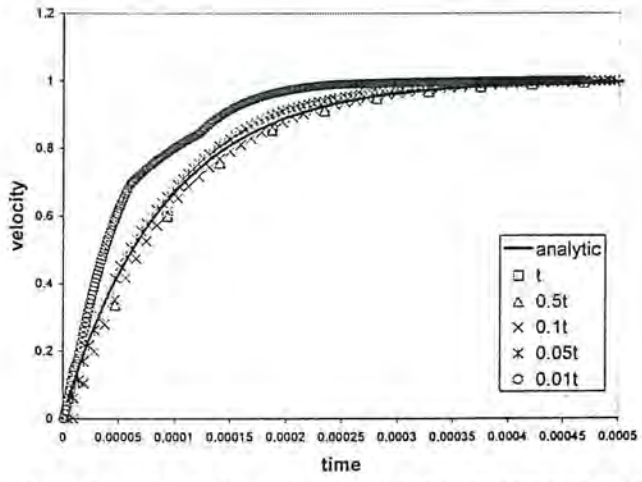

Figure 3. Comparison between the analytic and numerical solution for benchmark testing of the particle-tracking code; sim. 1.

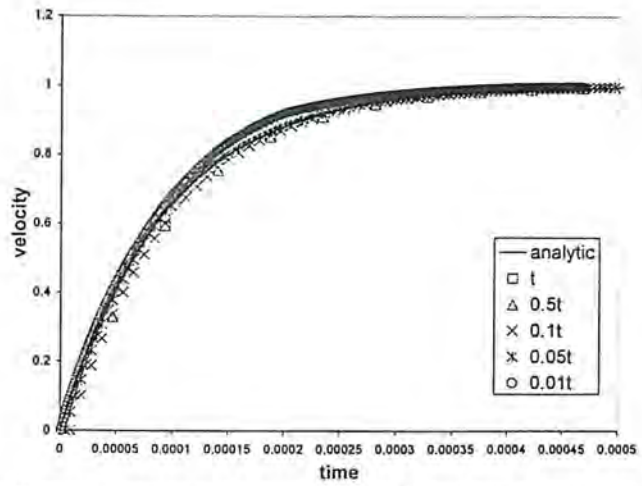

Figure 4. Comparison between the analytic and numerical solution for benchmark testing of the particle-tracking code; sim. 2.

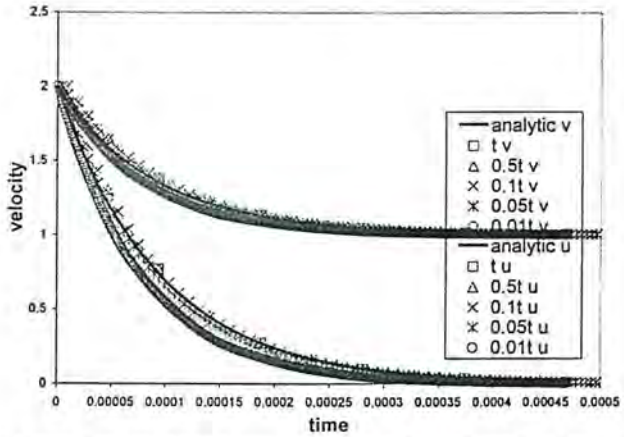

Figure 5. Comparison between the analytic and numerical solution for benchmark testing of the particle-tracking code; sim. 3.

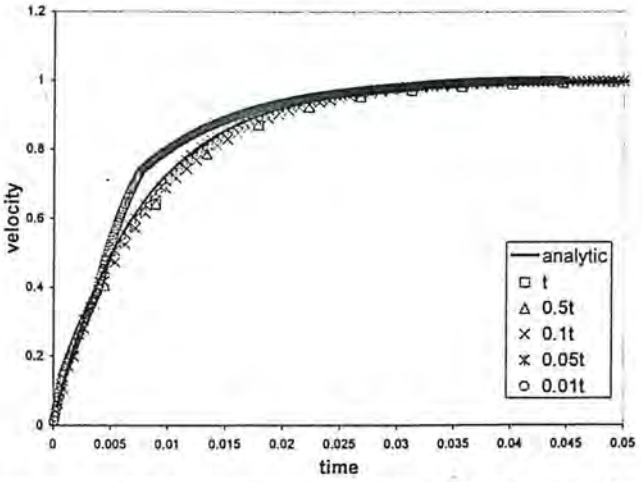

Figure 6. Comparison between the analytic and numerical solution for benchmark testing of the particle-tracking code; sim. 4.

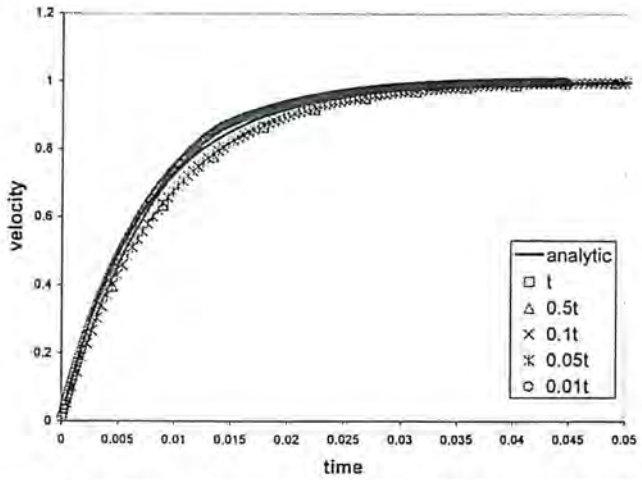

Figure 7. Comparison between the analytic and numerical solution for benchmark testing of the particle-tracking code; sim. 5.

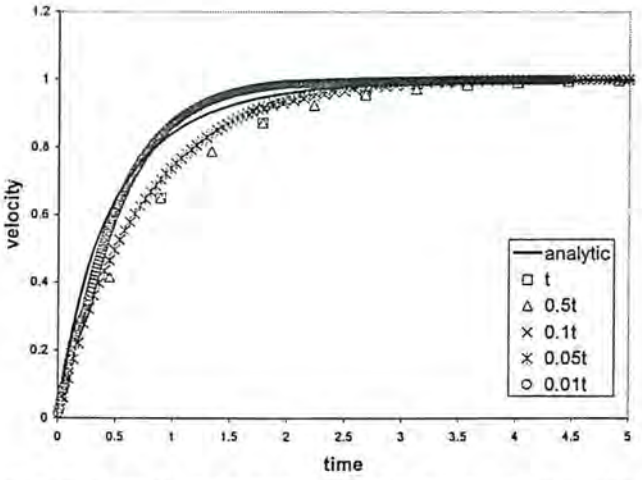

Figure 8. Comparison between the analytic and numerical solution for benchmark testing of the particle-tracking code; sim. 6.

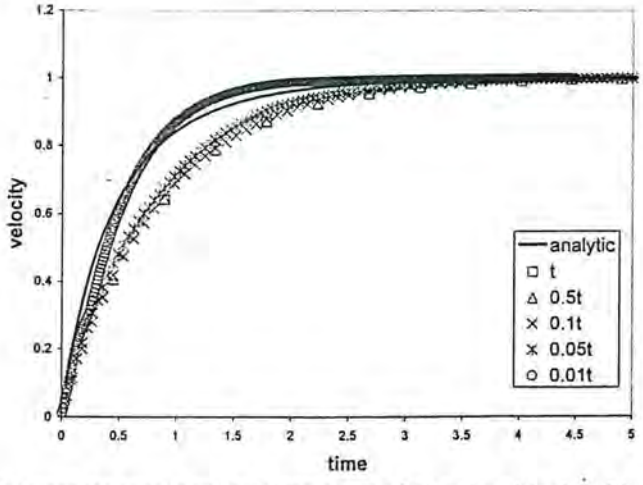

Figure 9. Comparison between the analytic and numerical solution for benchmark testing of the particle-tracking code; sim. 7.

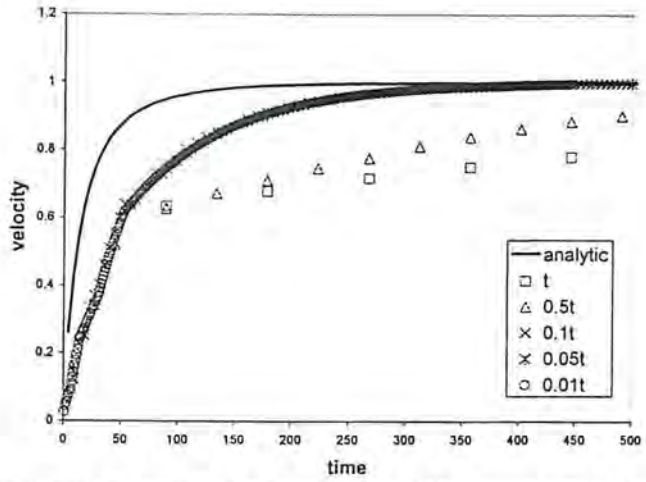

Figure 10. Comparison between the analytic and numerical solution for benchmark testing of the particle-tracking code; sim. 8.

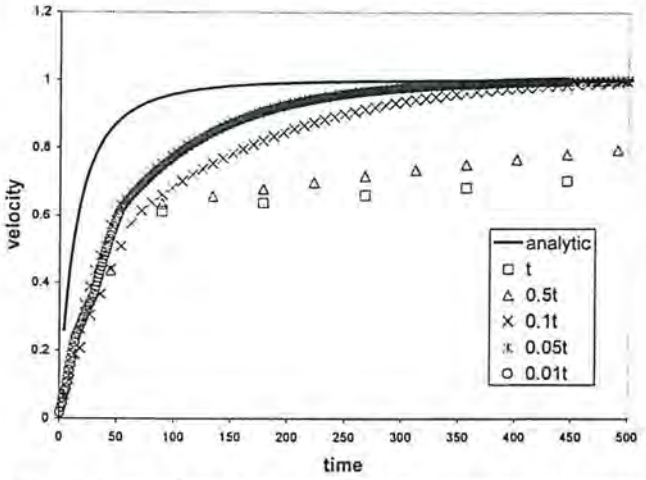

Figure 11. Comparison between the analytic and numerical solution for benchmark testing of the particle-tracking code; sim. 9.

In addition to examining the code's behavior with respect to change in Δt, it is also necessary to point out the accuracy of the code in predicting velocities for different particle sizes. It is clear from examination of the plots for d_p = 340 μm and d_p = 3400 μm, that considerable error with relative ∞-norms of 0.2 and 0.4, respectively, between the analytic and numerical solutions persist. These errors are considerably lower for d_p = 3.4 μm and d_p = 34 μm, each with relative ∞-norms of 0.1. These results indicate that, as particle size increases, and concurrently as the particles are less likely to follow the motion of the fluid, the particle tracking code becomes less accurate. It is also notable that for all particle sizes and for all Δt, the particle velocity eventually relaxes to that of the fluid; note that this is cut off for the 3400 μm particle graphs for $\Delta t = \tau$ and 0.5τ. Hence, the predominant source of error between particle and fluid velocities is during the time needed for relaxation to the fluid velocity.

Testing the Long-Time Behavior of the DVM: Results

Figures 12a-c display instantaneous velocity fields for simulations A-C at *Re* = *5,232* and t = 15 (non-dimensional time units). For simulation A, coherent eddies maintained their shape as they traveled downstream. When the input parameters were coarsened for simulations B and C, the eddies disappeared and only waves could be seen downstream. Figures 13a-c display the instantaneous velocity fields for simulations D-F at *Re* = 140,000 and t = 15. Coherent eddies were maintained downstream for simulations D and E, but those features were lost upon further coarsening.

Simulation	L_B	*Str*
A	0.610	0.211
B	0.526	0.213
C	0.581	0.217
D	0.447	0.224
E	0.463	0.217
F	0.557	0.216
G	0.843	0.190
Experiment	2.10	0.210

Table III. Discrete vortex method model output.

Table III displays simulation and experimental results for Strouhal number, *Str*, and time-averaged recirculation zone length, L_B. The experimental value for *Str* was in excellent agreement with measurements of *Str* vs. *Re* for *Re* < 10,000 taken by Roshko (1954) as *Str* = *0.21* and confirmed numerous times in the literature (Hinze, 1975). Calculations for *Str* for simulations A-C are in very good agreement with the experimental values. For *Re* = *140,000*, Cantwell & Coles summarised the experimental values found in the literature for *Str* and found that *Str* = *0.2*; only one significant figure is used here because there was more variability in the experimental data at this higher Reynolds number. There was reasonable agreement between the computed values of Strouhal number and the experimental values.

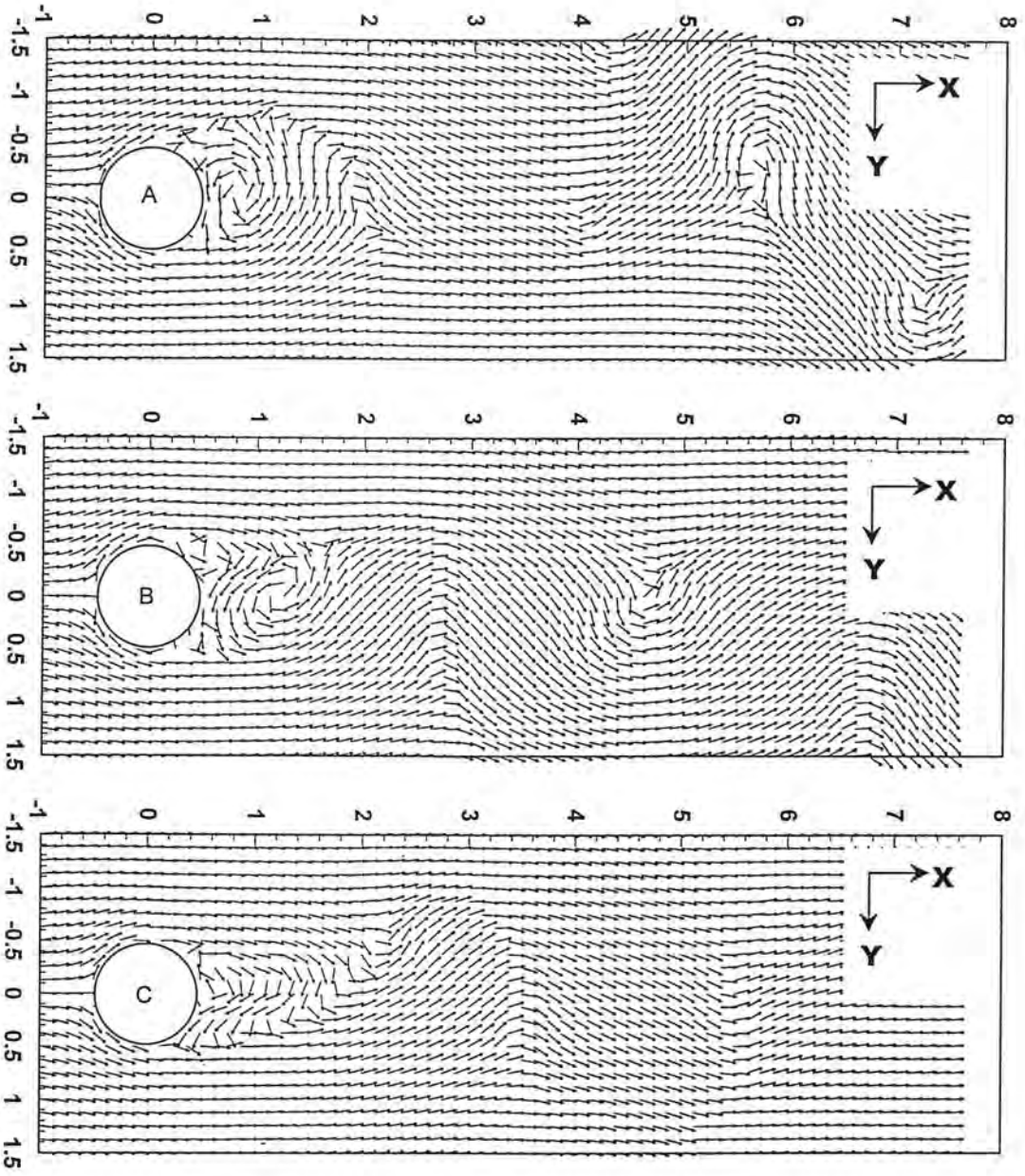

Figure 12. Instantaneous velocity field for *Re = 5,232*, *t* = 15. (a) $\Delta t = 0.0125$, (b) $\Delta t = 0.025$, (c) $\Delta t = 0.05$.

Figure 14 shows the time-averaged velocity field obtained experimentally over 330 shedding cycles for *Re = 5,232*. The experimentally-measured bubble length was 2.10. From the standard error of the stream-wise velocity at each sampling point, $1.59 \leq L_B \leq 2.42$. These findings are consistent with the range of $1.5 \leq L_f \leq 2.0$ (*Re = 5,000*, for measurements under 1.0% to 0.03% turbulence intensity, respectively) reported by Bloor (1964) for a formation length, L_f, defined as the point along the centerline where an instantaneous velocity contour first crosses after wrapping around one side of the cylinder. Bloor (1964) used hot-wire anemometry to measure formation length as the point along the centerline where there is a significant drop in turbulence intensity. Use of this measurement technique implies that Bloor (1964) actually located the time-averaged stagnation point at the edge of the

recirculation bubble and not a point of instantaneous change in the profile. Even if Bloor (1964) actually did measure the formation length, it would be expected that its value would be close to the time-averaged bubble length.

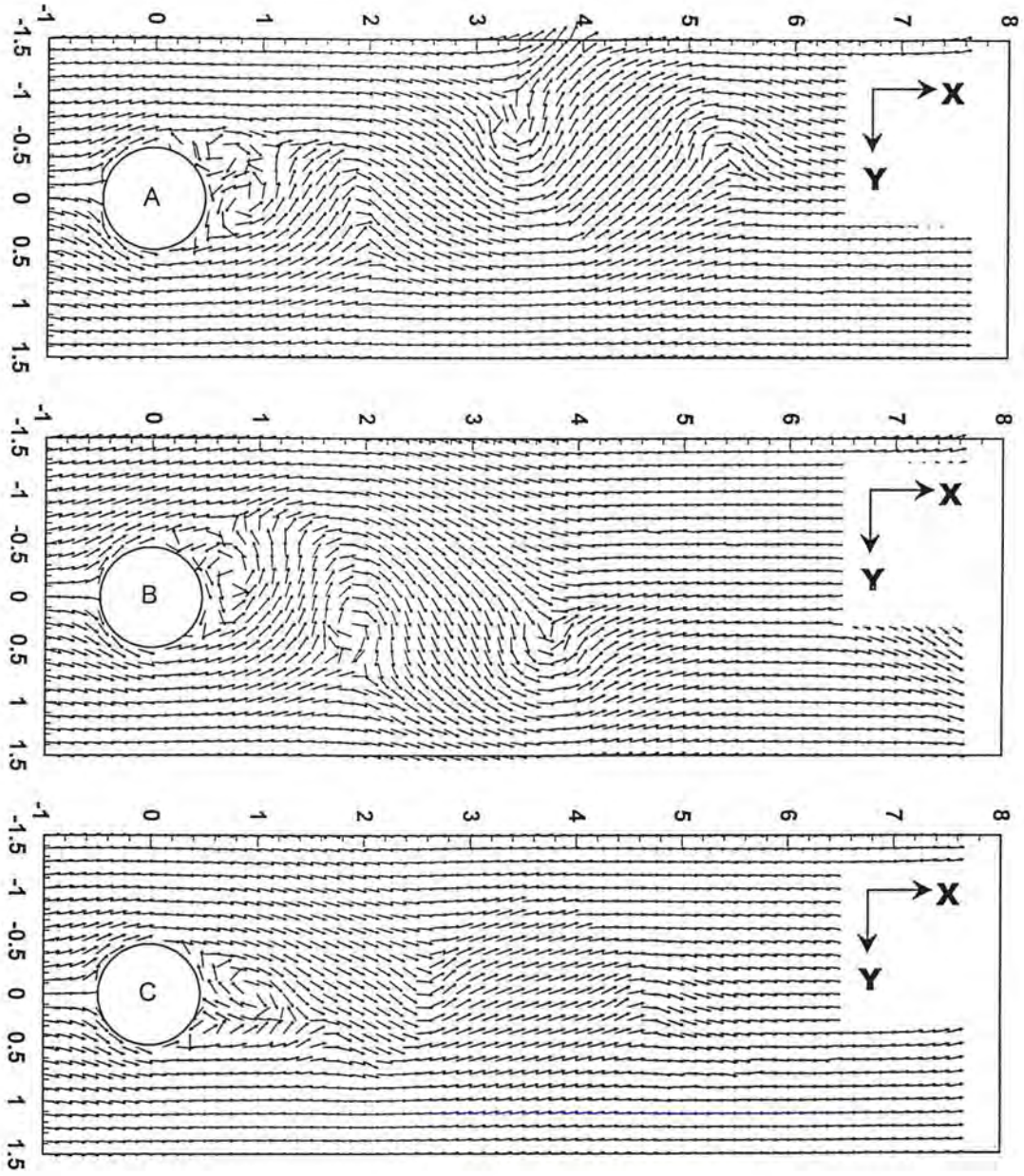

Figure 13. Instantaneous velocity field for *Re = 140,000*, $t = 15$. (a) $\Delta t = 0.0125$, (b) $\Delta t = 0.025$, (c) $\Delta t = 0.05$.

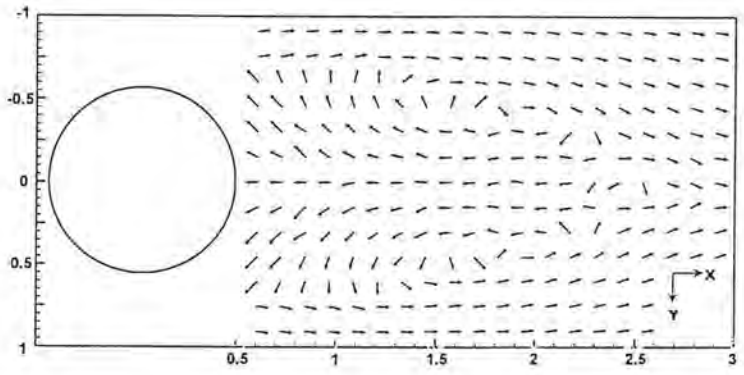

Figure 14. Experimental velocity vectory field for *Re = 5,232.*

L_B was calculated as the distance along the centerline from the base of the cylinder to the edge of the recirculation zone. It was computed at various times for each simulation and then time-averaged until it had stabilized. The L_B results were much different for the two *Re* tested in simulation. For *Re = 5,232*, no ostensible trend could be deduced for L_B upon parameter refinement. Even for the most refined simulation, L_B did not converge.

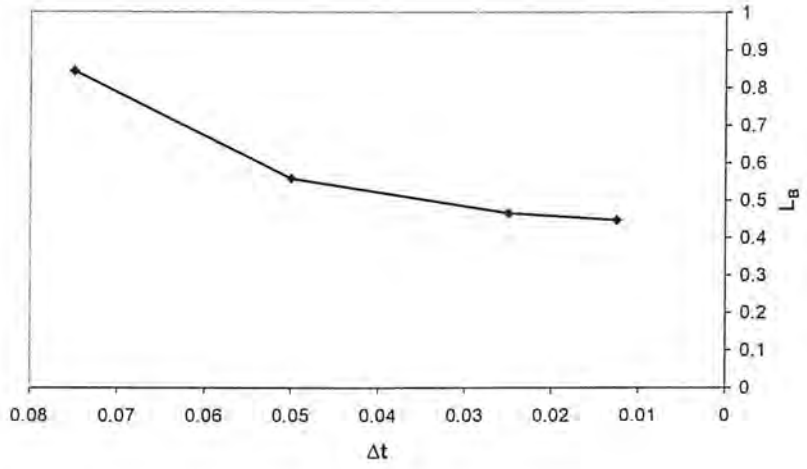

Figure 15. Change in bubble length with respect to time-step for Re = 140,000.

Results for the higher *Re* simulations were much more encouraging. Figure 15 plots L_B vs. Δt, once L_B had stabilized for each simulation. Clearly, L_B first decreases with Δt and then approaches a constant value of 0.45. Figures 16a and 16b display the time-averaged velocity vector profiles measured by Cantwell & Coles (1983) and computed in the simulation, respectively. In both cases, a small recirculation bubble is evident. Cantwell & Coles (1983) reported that the stagnation point at the end of the recirculation bubble was located 'slightly more than half a diameter downstream' of the stagnation point at the rear centre of the cylinder. In reasonable agreement, the average length of the time-averaged recirculation region was 0.447 diameters for the simulation. This stagnation point value is steady for 500 time-steps. The predicted time-averaged velocity field showed good agreement with experiment.

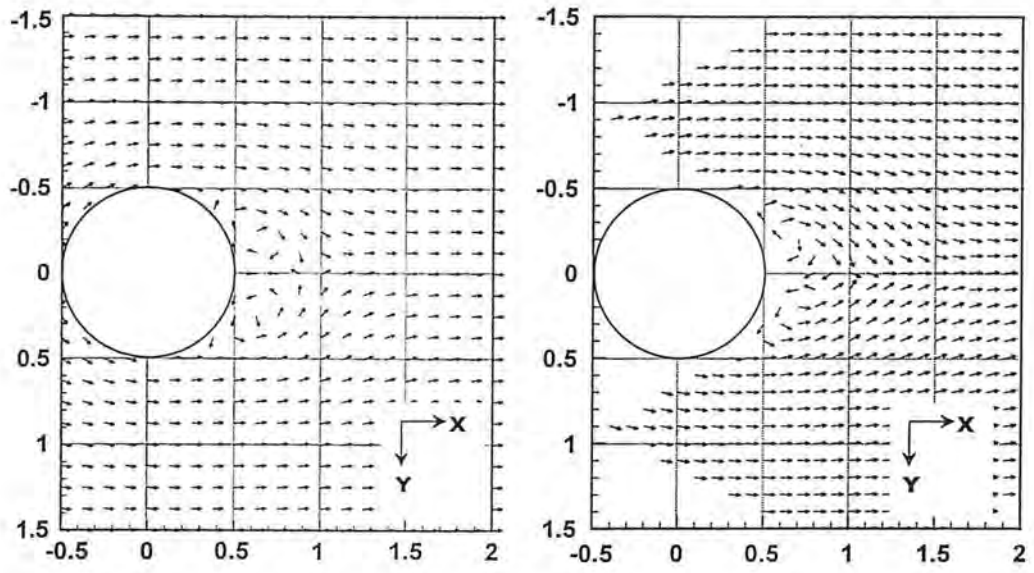

Figure 16. Time-averaged velocity for Re = 140,000. (a) Data from Cantwell & Coles (1983); (b) simulation.

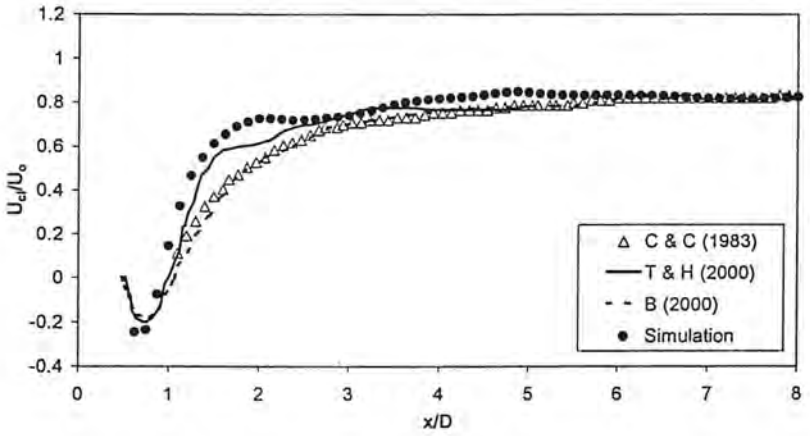

Figure 17. Comparison between centerline velocity profiles obtained from the simulation and from Cantwell & Coles (1983) (C&C), Tutar & Holdø (2000) (T&H), and Breuer (2000) (B).

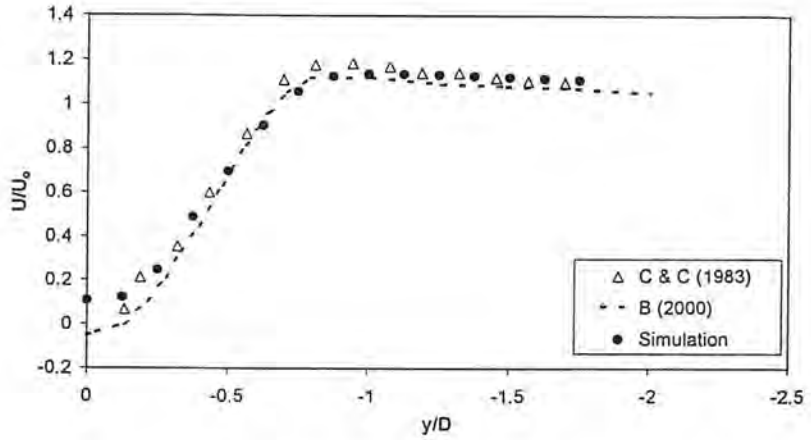

Figure 18. Comparison between shear velocity profiles, obtained at *x/D* = 1, from simulation and from Cantwell & Coles (1983) (C&C) and Breuer (2000) (B).

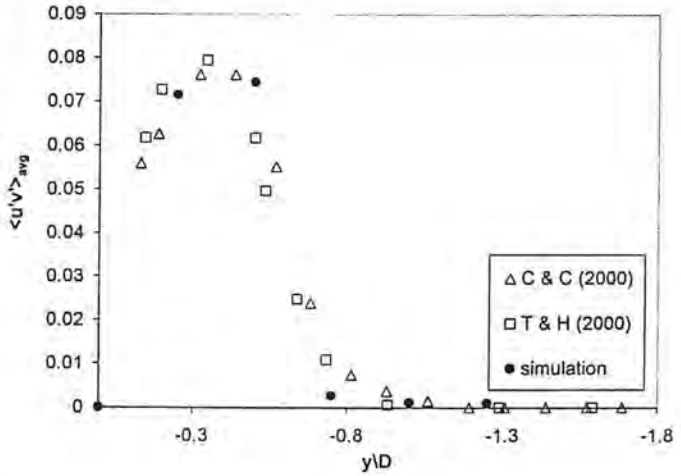

Figure 19. Comparison between shear stress profiles, obtained at *x/D* = 1, from simulation and from Cantwell & Coles (1983) (C&C) and Tutar & Holdø (2000) (T&H).

Figures 17, 18, and 19 compare the *Re = 140,000* simulation results with experimental data from Cantwell & Coles (1983), as well as with large eddy simulation (LES) results computed by Tutar & Holdø (2000) and by Breuer (2000). There is fair agreement between the experimental and simulated centerline velocity profile (figure 8). The primary discrepancy between this data occurs for $1 \leq x/D \leq 3$, where the velocity transitions from near-zero to that of the freestream; as $x/D \rightarrow \infty$, the centerline velocity for the simulation approached that of the experiment. Tutar & Holdø (2000) saw the same discrepancy, although Breuer's (2000) results matched Cantwell & Coles' (1983) data well. There is excellent agreement for the shear layer velocity profile (figure 18). For this, the simulation values always fall within one standard deviation of the experimental data. There is also reasonable agreement between the experimental and simulated shear stress profiles (figure 19). In this case, the simulated data lie well within the 95% confidence intervals around the experimental data.

Testing the Long-Time Behavior of the DVM: Discussion

The qualitative test for convergence to physical results was the appearance of shedding vortices. This requirement was met for both Reynolds numbers examined. Although shedding is a requirement for a physically-converged solution, Strouhal number is insufficient for a converged solution. As shown in Table II, there was little variability in the value of *Str* for either *Re* upon parameter refinement. Rodi et. al. (1997) and Breuer (1998) also observed this insensitivity of *Str* to changes in discretisation level. Rodi et. al. (1997) stated that, for this reason, *Str* is a poor indication of solution accuracy. The time-averaged length of the recirculation zone downstream of the cylinder, L_B, was considered the best quantitative measure of code verification because it was more sensitive to changes in input parameters.

There is strong evidence that a physically-converged solution can be attained for *Re = 140,000*. In figure 15, L_B approaches a constant value as $\Delta t \rightarrow 0$. Because shedding was maintained at $\Delta t = 0.025$ while the asymptotic time-averaged value of L_B is maintained, our definition of a verified solution is fulfilled. However, convergence with respect to L_B could not be demonstrated for *Re = 5,232*. Given the computational cost of this simulation (approximately 2000 CPU hours), continued study of the convergence properties of the DVM through parameter refinement at Re = 5,232 is prohibitive without massively-parallel resources and/or a multipole implementation. Breuer (2000) and Jordan & Ragab (1998) noted the need for spanwise resolution, presumably obtained from a three-dimensional simulation, to observe secondary eddies in the long time-averaged velocity field for their LES simulations for flow past a cylinder at Re = 3,900 and 5,600, respectively. They observed that a two-dimensional simulation results in overprediction of the base pressure coefficient on the cylinder. Moreover, Jordan & Ragab (1998) report experimental evidence that overprediction of the base pressure coefficient is strongly correlated with underprediction of the formation length. It is notable to mention that secondary eddies have been observed in two-dimensional simulations by Koumoutsakos & Leonard (1995) for Re = 3,000 and 9,500 and by Cheer (1989) for Re = 3,000, 9,500, and 10,000 during the highly-resolved simulations of the initial growth period of the bubble in a two-dimensional DVM simulation. Secondary vortex formation has not been demonstrated in the literature for a long-time vortex simulation.

This discussion leads to the question: why did we observe convergence to physical results at *Re = 140,000*? Because this higher-*Re* flow is less diffusive, there is no secondary eddy formation behind the cylinder. Although Cantwell & Coles' (1983) measurements were not sufficiently detailed at the edge of the cylinder to make this observation, it is clear from the two-dimensional LES results by Tutar & Holdø (2000) and from three-dimensional LES results by Breuer (2000) that no secondary eddies exist at this higher Reynolds number. Additionally, if the viscosity contributes to the overall error of the method for flows that include boundaries, the computational requirements for the lower-*Re* simulation would be substantially larger. Hence, attainment of the converged long-time solution becomes more feasible at higher-*Re*.

As for the verification study, the time-averaged velocity field provides the best comparative data set. While there was a good comparison with experimentally-computed Strouhal numbers for all simulations, these validations are less meaningful because some were made for non-verified simultions.

For the 600 time-step period prior to shedding, L_B grew to approximately 1.47 diameters long; the Re = 5,232 simulation appeared to fall just short of the experimental results for bubble length. However, once shedding began, the size of the shedding eddy cores shrank dramatically; this lead to the significant drop in bubble length. No validation can be made of the DVM at Re = 5,232 without investing significantly greater resources.

Encouragingly, validation could be made for the physically-converged *Re = 140,000* results. Good agreement was observed for point-wise time-averaged velocity results as well as for L_B. Discrepancies between the simulation and Cantwell & Coles' (1983) data were seen only for the centerline velocity profile. Based on the accuracy of the DVM at *Re = 140,000*, it might be postulated that there is systematic bias in the experimental data set causing this disparity between the near wake centerline profiles. However, this is a speculative statement because Breuer's (2000) results agreed with those of Cantwell & Coles (1983), while Tutar & Holdø's results were in accordance with ours. Slight differences also exist between the computed shear stress profile and that of Cantwell & Coles (1983). However, the uncertainty in the experimental data set for shear stress is greater than for the shear and centerline velocity profiles. This is natural because shear stress is a second-order term, which causes the error to propagate with each component of velocity (ASME, 1998). It is also important to note that, although data from other simulations cannot be used to validate the current simulation, they do lend confidence to the experimental data set used for validation. Data from the Tutar & Holdø (2000) and Breuer (2000) studies are therefore included in figures 8, 9, and 10 for comparative purposes.

These results have strong implications for modelers in industrial hygiene applications. For the lower Reynolds numbers studied in this exercise, time-averaged concentrations may be in error if the dispersed phase follows the fluid movement exactly. Given the quality of the high Reynolds number results, this type of error would not be anticipated for these flows. However, instantaneous profiles may be well-represented in both cases. Furthermore, it is also possible that the time-averaged profile of the transport phase may be dominated by shedding phenomena or by L_f rather than by the time-averaged air velocity profile. If this is the case, application of vortex methods to the study of time-averaged particle concentrations may not be Reynolds number dependent. This test will be made in continued study of the long-time behavior of the particle-tracking DVM.

Additionally, the process followed in this exercise suggests that a rigorous study of the convergence characteristics of a CFD method is essential to understanding the applicability of the results. Without such fastidiousness, it is possible for the applied modeler to derive a mistaken conclusion from simulation output. For example, there is an 17% relative error in L_B for *Re = 140,000* between $\Delta t = 0.05$ and $\Delta t = 0.025$. Failure to refine the input parameters would then lead to the conclusion that the size of the area where contaminants could be brought within the breathing zone is also 17% larger, based on the approximation that the width of this region is determined only by the width of the body. This could potentially lead to overprediction of exposure, if a contaminant source is brought within the recirculation zone, or to underprediction, if the contaminant source is outside this zone.

Development and Testing of the Particle-Tracking Module of the DVM: Experimental Results and Discussion

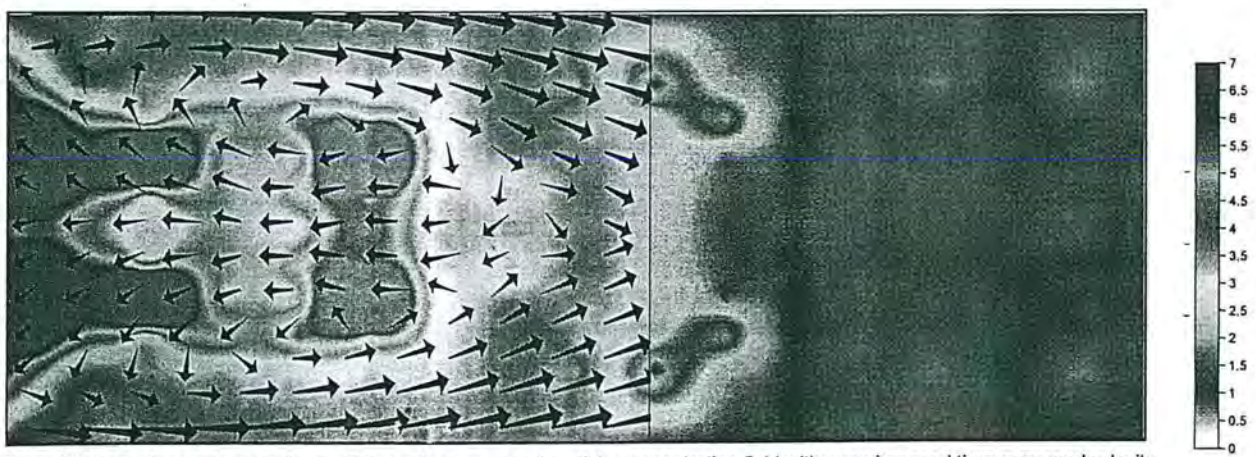

Figure 20. Experimental results for the 3.4 μm time-averaged particle concentration field with superimposed time-averaged velocity field.

Figure 20 shows the experimental time-averaged particle concentration field for 3.4 μm particles released far upstream of the cylinder. Concentration levels have been normalized with respect to the freestream time-averaged particle concentration. The time-averaged velocity field is superimposed over the concentration field to illustrate how the fluid motion corresponds with the areas of high and low concentration. With respect to the flow, the domain can be divided into the near wake region (i.e. the recirculation zone), the region at the base of the recirculation zone where the streamlines converge, and the region further downstream of the near wake region. In the recirculation zone, it is evident that there are high peaks in the concentration immediately behind the cylinder and near the center of recirculation of the time-averaged eddies. A second, smaller peak is evident at the convergence located at the end of the recirculation zone. Farther downstream from the cylinder, the concentration diminishes. Jacober and Matteson (1990) saw a similar peak at the edge of the recirculation zone for small particle transport experiments with flow past a sphere.

It is possible that the concentration peaks within the recirculation zone are actually an artifact of the manner in which the concentration, C, is extracted from the velocity output generated by the PDA signal processor:

$$C = \frac{1}{AT}\sum_{i-1}^{N}\frac{1}{U_i} \qquad (3)$$

where A = area of the photodetector aperture
T = total sampling time
U = particle velocity
N = total number of particles registered during the sample.

Considering A and T to be constant, the concentration depends directly on N and inversely on U_i. Given that some particles move with near-zero velocity within this region, these low velocities dominated the near wake concentration even when there were very few particles in this zone. The second, smaller, concentration peak corresponded to a greater number of particles and, concurrently, to a stagnation region in the flow. It is likely that this is a real feature of the flow, rather than an artifact of the measurement technique. Finally, the reduction in concentration further downstream may merely signify a return to freestream conditions.

Development and Testing of the Particle-Tracking Module of the DVM: Preliminary Simulation Results

The DVM code was amended to implement particle motion through the driver code of the routine. At a user-designated time after vortex shedding first occurs, two options are available for the user to choose. The "Stokes" option contains three do loops to diffuse, convect, and diffuse each particle. Diffusion is computed with a random walk whose standard deviation is based on the particle coefficient of diffusion. It is implemented in two half steps, in the same manner as is done for the fluid. Particle convection is computed by finding the air velocity at the location of the particle, based on the assumption that they are the same for very small particles. The "Non-Stokes" option varies in that the convection routine is a BDF integration of the particle equation of motion (Hindmarsh, 1980). In either case, if particles encounter the cylinder, they are reflected off the body of the cylinder and back into the freestream. Next, the location of each particle is logged. Then, the concentration routine is invoked to superimpose a grid over the domain. In each cell of the grid, the number of particles is counted and factored into a time-averaged concentration.

Because it was determined that a large effort was necessary for determining the long-time convergence characteristics of the airflow model prior to determining the limitations of the particle-tracking module, convergence testing for the particle portion of the code was minimal. More rigorous testing is planned for the near future. However, some preliminary tests have been performed and are presented here.

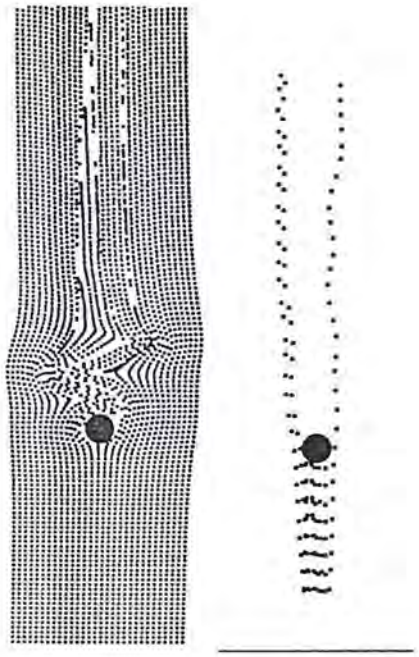

Figure 21. Particle streak lines for simulations with Stokes numbers of 5.9×10^{-7} (left) and 5 (right).

Figure 21 displays two streak plots for particles released upstream of the cylinder into a shedding flow. Both of these simulations were preliminary in nature and run before the fluid model convergence test was performed. However, these plots do display that the code adequately distinguishes between particle behavior at very low Stokes numbers, where the particles disperse everywhere, and high Stokes numbers, where the particles either impact the cylinder or are unaffected by the motion of the eddies. Additionally, the behavior of particles with respect to injection site was investigated. These results were published in publication #1, which is reproduced for this report in the Appendix.

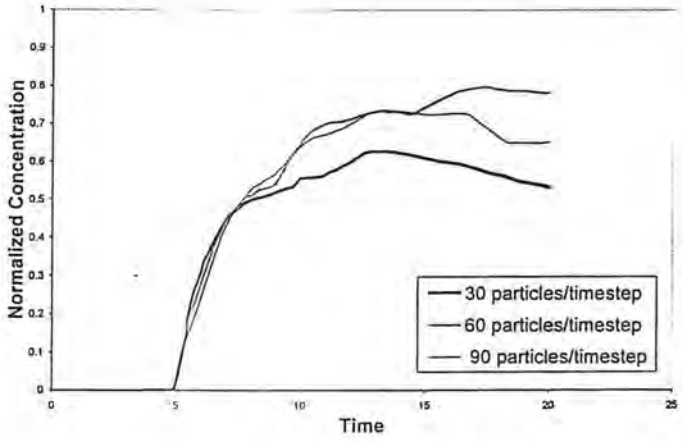

Figure 22. Time-averaged concentrations for 30, 60, and 90 particles in a 1 x 1 square located one diameter downstream of the cylinder.

Although the time needed for the time-averaged concentration throughout the domain is very long, the concentration stabilizes more quickly in the region immediately downstream of the cylinder. Figure 22 shows the time-averaged concentration in a 1x1 box located one diameter downstream when 30, 60, and 90 particles are released ten diameters upstream of the cylinder along a 6D line during each time

step. At t = 15, it appears that there is no difference between the 60 and 90 particle simulations. However, a discrepancy, growing to 16%, becomes evident hereafter but then appears to level off.

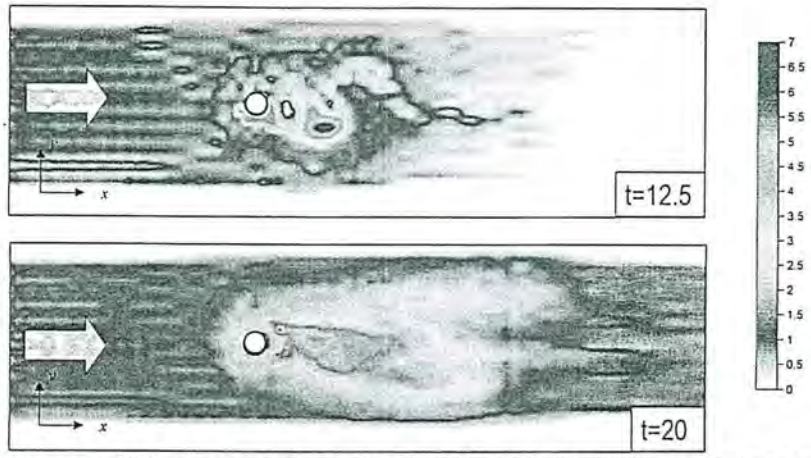

Figure 23. Time-averaged 3.4 μm concentration profile at t = 12.5 and t = 20. Particles are first released into the airstream once shedding has begun, at t = 10.

Time-averaged concentrations were examined in more detail for the low-Stokes number case shown in figure 23. Again, it should be noted that the airflow was not fully tested for convergence at this point; furthermore, there was a small error in the code that was detected and subsequently repaired after this run was completed. However, because the flow field displayed the correct qualitative time-averaged and instantaneous features, it is acceptable for preliminary discussion. This simulation will be re-run shortly.

At low Stokes numbers, it is expected that the particles follow the airflow exactly. However, this would imply that the particles will concentrate everywhere uniformly. In contrast, we see in figure 23 that, 2.5 seconds after the particles are released into the freestream (t = 12.5), the concentration pattern closely resembles the eddy dispersion pattern. This implies that the small particles can become trapped inside the moving eddies. However, at t = 20, the region of peak concentration begins at the edge of the recirculation zone and extends further downstream into the far wake.

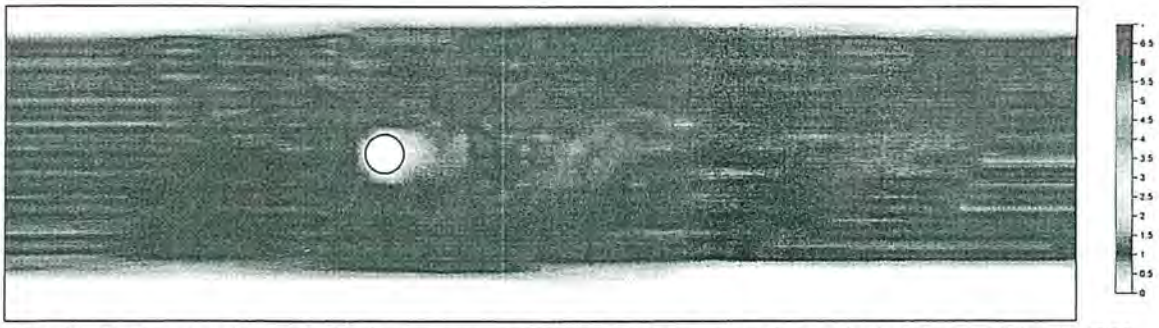

Figure 24. Time-averaged concentration for tracer gas, released under the same conditions as for the 3.4 μm particles, t = 16.25.

In order to distinguish between the behavior of small particles and of the fluid, a second simulation with tracer gas was performed. All other conditions were the same as for that presented in figure 23. For the tracer gas, the concentration was uniform everywhere. Knowing that the convective velocity was the same for the 3.4 μm particles as it was for the tracer gas, there is only one possibility to explain this disparity. The tracer gas diffuses instantaneously into the air, while the particle diffusion is slower. This does not explain the specific pattern of particle dispersion in the simulation. However, there was some commonality between the experimental and numerical time-averaged particle concentrations. In both cases, there was a peak in concentration located at the edge of the recirculation zone. It is also very important to mention that these simulations have not run until the particle concentration has reached

equilibrium everywhere in the domain. Until this occurs, no substantive statement can be made regarding the observed results.

If this observation regarding the peak concentration area at the base of the recirculation zone is correct, then for particles released upstream of the worker, the highest concentrations are farther away from the body. Therefore, they are away from the breathing zone. However, the simulation output did show some elevation with respect to the freestream in the breathing zone concentration. This may be an artifact of the designation that the body does not collect particles in these simulations; the particles bounce back into the freestream if they encounter the cylinder. Hence, these simulations imply but show no conclusive evidence that worker exposure to small particles released upstream will be higher than the freestream concentration. It is hoped that these phenomena will be revealed in future planned simulations with the code developed here.

Chapter 5

References

American Institute of Aeronautics and Astronautics. (1998) *Guide for the Verification and Validation of Computational Fluid Dynamics Simulations.* AIAA-G-077-1998. Washington, DC.

American Society of Mechanical Engineers. (1998) *Test Uncertainty: Instruments and Apparatus. Supplement to ASME Performance Test Codes.* ASME PTC 19.1-1998. New York.

Anderson CR, Greengard C, Greengard L, Rokhlin V. (1990) "On the Accurate Calculation of Vortex Shedding." *Phys. Fluids A., Vol. 2.* Pp. 883-885.

Anderson DA, Tannehill JC, Pletcher RH. (1984) *Computational Fluid Mechanics and Heat Transfer.* Washington, DC: Hemisphere Publishing Corp.

Andersson I-M, Marttinem K, Niemela R, Rosen G, Raisanan J, Welling I. (1997) "Contaminant Dispersion Near a Worker in a Uniform Velocity Field." *Proceedings of the 5th International Symposium on Ventilation for Contaminant Control.* Ottawa, Canada. 14-17 September, 1997.

Bloor SM. (1964) "The Transition to Turbulence in the Wake of a Circular Cylinder." *J. Fluid Mech.* 19: 290-304.

Breuer M. (1998) "Large Eddy Simulation of the Subcritical Flow Past a Circular Cylinder: Numerical and Modeling Aspects." *Int. J. Numer. Meth. Fluids.* 28: 1281-1302.

Breuer M. (2000) "A Challenging Test Case for Large Eddy Simulation: High Reynolds Number Circular Cylinder Flow." *Int. J. Heat Fluid Flow.* 21: 648-654.

Brohus H. (1997) "CFD Simulation of Personal Exposure to Contaminant Sources in Ventilated Rooms." *Proceedings of the 5th International Symposium on Ventilation for Contaminant Control.* Ottawa, Canada. 14-17 September, 1997.

Cantwell B, Coles, D. (1983) "An Experimental Study of Entrainment and Transport in the Turbulent Near Wake of a Circular Cylinder." *J. Fluid Mech.* 136: 321-374.

Cheer AY. (1983) "Numerical Study of Incompressible Slightly Viscous Flow Past Blunt Bodies and Airfoils." *SIAM J. Sci. Stat. Comput.* 4: 685-705.

Cheer AY. (1989) "Unsteady Separated Wake Behind an Impulsively Started Cylinder in Slightly Viscous Fluid." *J. Fluid Mech.* 201: 485-505.

Chorin AJ. (1973) "Numerical Study of Slightly Viscous Flow." *J. Fluid Mech.* 57(4): 785-796.

Chorin AJ. (1978) "Vortex Sheet Approximation of Boundary Layers." *J. Comp. Phys.* 27: 428-442.

Chorin AJ. (1980) "Vortex Models and Boundary Layer Instability." *SIAM J. Sci. Stat. Comp.* 1(1): 1-21.

Drain LE. (1972) "Coherent and Noncoherent Methods in Doppler Optical Beat Velocity Measurement." *J. Phys. D: Appl. Phys.* 5: 481-495.

Dunnett SJ. (1994) "A Numerical Investigation Into the Flow Field Around a Worker Positioned by an Exhaust Opening." *Ann. Occup. Hyg.* 38(5): 663-686.

Durst F, Whitelaw JH. (1971) "Optimization of Optical Anemometers." *Proceedings of the Royal Society of London A.* 324: 157-181.

Flynn MR, Chen MM, Kim T, Muthedath P. (1995) "Computational Simulation of Worker Exposure Using a Particle Trajectory Method." *Ann. Occup. Hyg.* 39(3): 277-289.

Flynn MR, George DK. (1991) "Aerodynamics and Exposure Variability." *Appl. Occup. Environ. Hyg.* 6(1): 36-39.

Flynn MR, Miller CT. (1991) "Discrete Vortex Methods for the Simulation of Boundary Layer Separation Effects on Worker Exposure." *Ann. Occup. Hyg.* 35(1): 35-50.

Foreman JW, George EW, Lewis RD. (1965) "Measurement of Localized Flow Velocities in Gases with a Laser Doppler Flowmeter." *Appl. Phys. Letters.* 7(4): 77-78.

George DK, Flynn MR, Goodman R. (1990) "The Impact on Boundary Layer Separation on Local Exhaust Design and Worker Exposure." *Appl. Occup. Environ. Hyg.* 5(8): 501-509.

George WK. (1979) "Processing of Random Signals." *Dynamic Meas. In Unsteady Flows., Proceedings of the Dynamic Flow Conference.* Skovlunde, Denmark.

Ghoniem AF, Chorin AJ, Oppenheim AK. (1982) "Numerical Modelling of Turbulent Flow in a Combustion Tunnel." *Phil. Trans. R. Soc. Lond. A.* 304: 303-325.

Guffey SE, Barnea N. (1994) "Effects of Face Velocity, Flanges, and Mannikin Position on the Effectiveness of a Benchtop Enclosing Hood in the Absence of Cross-Drafts." *Am. Ind. Hyg. Assoc. J.* 55: 132-139.

Helgeson JK. (1992) *Particle Mixing and Diffusion in the Turbulent Wake of Cylinder Arrays.* Ph.D. Thesis, Georgia Institute of Technology, Atlanta.

Heist DK, Richmond-Bryant J, Eisner A, Conner T. (2001) "Development of a Versatile Aerosol Generation System for Use in a Large Wind Tunnel." Submitted for publication in *Aerosol Sci. Tech.*

Hindmarsh A. (1980) "LSODE and LSODI, Two New Initial Value Ordinary Differential Equation Solvers." *ACM—Signum Newsletter.* 15(4): 10-11.

Hinze JO. (1975) *Turbulence, 2nd Edition.* New York: McGraw-Hill.

Høst-Madsen A, Caspersen C. (1994) "The Limitations in High Frequency Turbulence Spectrum Estimation Using the Laser Doppler Anemometer." *Seventh International Symposium on Applications of Laser Techniques to Fluid Mechanics.*

Ibrahim KM, Wertheimer GD, Bachalo WD. (1990) "Signal Processing Considerations for Laser Doppler and Phase Doppler Applications." *Applications of Laser Techniques to Fluid Mechanics, 5th International Symposium*, Lisbon, Portugal.

Jacober DE, Matteson MJ. (1990) "Particle Mixing and Diffusion in the Turbulent Wake of a Sphere." *Aerosol Sci. Tech.* 12: 335-363.

Jordan SA, Ragab, SA. (1998) "A Large Eddy Simulation of the Near Wake of a Circular Cylinder." *J. Fluids Eng.* 120: 243-252.

Koumoutsakos P, Leonard A. (1995) "High-Resolution Simulations of the Flow Around an Impulsively Started Cylinder Using Vortex Methods." *J. Fluid Mech.* 296: 1-38.

Kulmala I, Saamanen A, Enbom S. (1996) "The Effect of Contaminant Source Location on Worker Exposure in the Near-Wake Region." *Ann. Occup. Hyg.* 40(5): 511-523.

Lading L. (1973) "Analysis of Signal-to-Noise Ratio of the Laser Doppler Velocimeter." *Optoelectronics.* 5: 175-187.

Launder BE, Spalding DH. (1974) "The Numerical Computation of Turbulent Flows." *Computer Methods in Applied Mechanics and Engineering.* 3: 268-289.

Michaelides EE. (1997) "Review—The Transient Equation of Motion for Particles, Bubbles, and Droplets." *J. Fluids Eng.* 119(2): 233-247.

National Institute for Occupational Safety and Health. (1991) *Building Air Quality: A Guide for Building Owners and Facility Managers.* Cincinnati, OH: U.S. Department for Health and Human Services, Public Health Service, Centers for Disease Control, National Institute for Occupational Safety and Health, DHHS (NIOSH) Publication No. 91-114.

Rodi W, Ferziger JH, Breuer M, Pourquié M. (1997) "Status of Large Eddy Simulation: Results of a Workshop." *From the Workshop on LES of Flows Past Bluff Bodies, Rottach-Egern, Tegernsee, Germany, June 26-28, 1995. J. Fluids Eng.* 119: 248-262.

Roshko A. (1954) "On the Development of Turbulent Wakes from Vortex Streets." *Report 1191 for the National Advisory Committee for Aerodynamics (NACA).*

Rudd MJ. (1969) "A New Theoretical Model for the Laser Dopplermeter." *J. Sci. Instr.* 2(2): 55-58.

Saamanen AJ, Kulmala IK, Enbom SA. (1998) "Control of Exposure Caused by a Contaminant Source in the Near Wake Region" *Appl. Occup. Environ. Hyg.* 13(10): 719-726.

Schlichting H. (1979) *Boundary Layer Theory.* New York: McGraw-Hill, Inc.

Sethian JA, Ghoniem AF. (1988) "Validation Study of Vortex Methods." *J. Comput. Phys.* 74(2): 283-317.

Soderholm SC. (1989) "Proposed International Conventions for Particle Size-Selective Sampling." *Ann. Occup. Hyg.* 33(3): 301-320.

Soutar CA, Miller BG, Gregg N, Jones AD, Cullen RT, Bolton RE. (1997) "Assessment of Human Risks from Exposure to Low Toxicity Occupational Dusts." *Ann. Occup. Hyg.* 41(2): 123-133.

Tiemroth EC. (1986) *The Simulation of the Viscous Flow Around a Cylinder by the Random Vortex Method (Ph.D. Dissertation).* University of California, Berkeley.

Tutar M, Holdø AE. (2000) "Large Eddy Simulation of a Smooth Circular Cylinder Oscillating Normal to a Uniform Flow." *J. Fluids Eng.* 122(4): 694-702.

Winter AR, Graham LJW, Bremhorst K. (1991) "Velocity Bias Associated with Laser Doppler Anemometer Controlled Processors." *J. Fluids Eng.* 113(2): 250-255.

Witschi HR, Last JA. (1996) "Toxic Responses in the Respiratory System." *Casarett & Doull's Toxicology (5th Ed.).* Ed. CD Klaassen. New York: McGraw-Hill, Inc.

Chapter 6

Publications

1) Richmond-Bryant J, Flynn MR. 2000 "Predicting Breathing Zone Concentrations of Aerosols Dispersed in a Time-Dependent Airflow Using Vortex Methods." *6th International Symposium on Ventilation for Contaminant Control.* 4-7 June 2000; Helsinki, Finland.

2) Richmond-Bryant J, Flynn MR. 2001 "Verification and Validation of a Discrete Vortex Method for Predicting Unsteady and Time-Averaged Flow Patterns." Submitted to *Journal of Fluids Engineering.*

3) Richmond-Bryant J, Flynn MR. 2001 "On the Effects of Diffusion on Small Particle Transport in a Structured Flow." Under preparation for submission to *Journal of Aerosol Science.*

4) Richmond-Bryant J, Flynn MR. 2001 "A Comparative Study of Computational Fluid Dynamics Models for Industrial Hygiene Applications." Under preparation for submission to *Annals of Occupational Hygiene.*

Appendix

From: *6th International Symposium on Ventilation for Contaminant Control.* 4-7 June 2000, Helsinki, Finland.

Predicting Breathing Zone Concentrations of Aerosols Dispersed in a Time-Dependent Airflow Using Vortex Methods

Richmond-Bryant J A, Flynn M R
CB #7400, Department of Environmental Science and Engineering, University of North Carolina, Chapel Hill, NC, USA

Introduction

When a person works facing a local exhaust ventilation (LEV) hood, it may be possible to obtain higher concentrations of aerosols in the breathing zone (BZ) than without the hood because recirculating eddies form downstream of the body. These eddies shed periodically in an alternating pattern called vortex shedding, which is thought to be a primary determinant of contaminant transport in and out of the breathing zone (1, 2, 3). Previous computational fluid dynamics (CFD) studies have explored the effect of time-dependent airflow on occupational exposure to gaseous contaminants (2, 3). However, none have employed CFD to assess occupational exposure to aerosols in a periodic air stream. In the present study, a two-dimensional Discrete Vortex Method (DVM) is used in conjunction with a Lagrangian particle-tracking algorithm to model this situation; particle number concentrations are then computed over a computational breathing zone.

Methods

A two-dimensional DVM was utilized to model the time-dependent airflow field. The DVM treats the fluid as convecting elements of vorticity and employs random walks on each element to simulate turbulent diffusion (4, 2, 3). Specific details about implementation of the method can be found in the literature (4, 5, 6). A 1-m circular cylinder represented the worker; although this size exceeds that of a typical worker, this diameter was used to non-dimensionalize the Navier-Stokes equations of fluid motion. The Reynolds number was set at 10,000 to yield a fluid velocity of 2.46×10^{-1} m/s. A timestep of 0.13 s was employed, and the simulation was run for 1600 timesteps, or 208 s.

A Lagrangian inertial particle-tracking algorithm ran in conjunction with the DVM. During each fluid timestep, the equation of particle motion due to drag forces was integrated several times with an adaptive timestep Backwards Difference Formulae method. Particles having Stokes numbers (Stk) of 1.87×10^{-4}, 4.63×10^{-3}, 1.16×10^{-1}, 1.00, and 5.00 were released at ten evenly-spaced points, from $x = -5.0 \times 10^{-1}$ m to $x = 5.0 \times 10^{-1}$ m, in separate simulations at $y = 7.5 \times 10^{-1}$ m, $y = 1.0$ m, and $y = 1.5$ m downstream of the cylinder center, which was centered at (0, 0). Ten particles were released per timestep, beginning at the 100-th timestep ($t = 13$ s). Figure 1 illustrates the initial conditions of particle release. The particle injection source velocity was zero; thus, particles initially follow the fluid motion. Particle concentration was calculated following a method proposed in (8). A grid containing 2816 square elements was

superimposed over the domain for the region x = −2.0 m to x = 2.0 m and y = −1.0 m to y = 10 m. Time-averaged concentrations were computed in a sub-domain from x = -5.0×10^{-1} m to x = 5.0×10^{-1} m and y = 0 m to y = 1.0 m; this sub-domain is comparable to the BZ. The designated BZ is also shown in Figure 1.

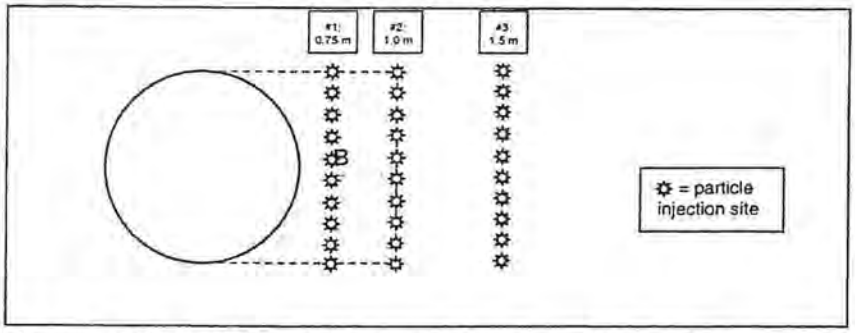

Figure 1. Schematic of the initial particle injection locations and breathing zone.

Results and Discussion

Figure 2 demonstrates the effect of particle release position on the time-averaged concentration for Stk = 1.16×10^{-1}. Simulations with other particle sizes produced similar results. BZ concentrations for the downstream release site of 7.5×10^{-1} m do not vary greatly with Stk. No consistent pattern between particle size and concentration level was observed. However, after this 208-s simulation, the time-averaged concentrations still have not reached steady-state values; hence, no conclusion can be drawn about the dependence of concentration on particle size. Accumulation of particles in the BZ is very noticeable for this set of runs because the site of particle injection lies within the BZ. Particles are injected into the domain faster than they can be effectively cleared from this region.

For the downstream release position of 1.0 m, BZ concentrations computed over the simulation time are lower than for the release position of 7.5×10^{-1} m. For any Stk, some accumulation of particles in the BZ occurs, although it is at a slower rate than for the 7.5×10^{-1} m injection site. It does appear that the Stk = 4.63×10^{-3} particles yield slightly higher BZ concentrations than do particles of other sizes. Stk = 1.87×10^{-4} and Stk = 1.16×10^{-1} particles have the next highest concentrations, followed by Stk = 1.00 and Stk = 5.00. It is intuitive that larger particles will be cleared from the BZ at a faster rate and thus will yield lower concentrations. However, as is the case for the 7.5×10^{-1} m injection site, the time-averaged number concentrations have not reached steady-state values, and therefore, any conclusions about the long-term concentration levels are premature.

In contrast with results from the other two injection positions, particle accumulation and overall concentration levels stabilize after some number of timesteps for the downstream release position of 1.5 m. A steady-state concentration level is then maintained for all Stk considered except Stk = 4.63×10^{-3}. At the release point of 1.5 m downstream of the cylinder, particles may either be reentrained into the recirculating bubble formed immediately downstream of the cylinder or they may be transported further downstream by the eddy which is being shed concurrently. This time-dependent behavior may explain why no clear relationship between BZ concentration and Stk can be garnered from these steady-state concentrations.

Conclusions

The most significant conclusion from this work is that the rate of accumulation of particulate matter within the BZ is strongly dependent upon the distance between the contaminant source and the body. The results also suggest that particle concentration levels within the BZ may also rely heavily on source distance; however, it is impossible to draw any strict conclusions about this relationship until steady-state concentrations have been attained. Simulations with $7.5x10^{-1}$ m and 1.0 m injection sites must be run for a longer period of time. No clear relationship between particle size and concentration level could be discerned from the results.

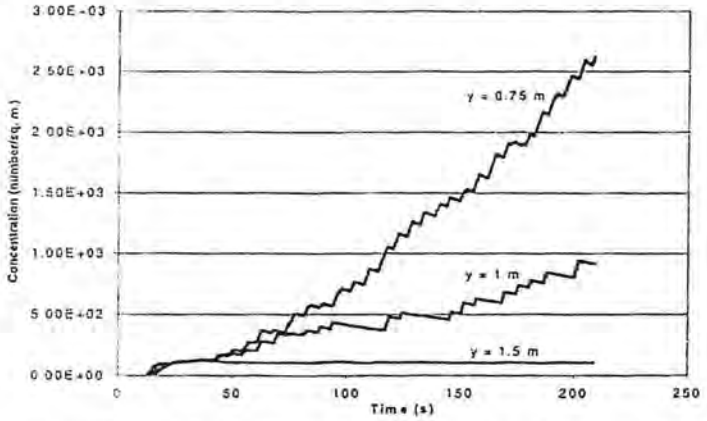

Figure 2. Time-averaged particle number concentration for Stk = $1.16x10^{-1}$.

References

1. Cantwell B, Coles, D. An Experimental Study of Entrainment and Transport in the Turbulent Near Wake of a Circular Cylinder. J. Fluid Mech 1983; 136: 321–374.
2. Flynn MR, Miller CT. Discrete Vortex Methods for the Simulation of Boundary Layer Separation Effects on Worker Exposure. Ann. Occup. Hyg, 1991; 35(1): 35–50.
3. Flynn MR, Chen MM, Kim T, Muthedath P. Computational Simulation of Worker Exposure Using a Particle Trajectory Method. Ann. Occup. Hyg. 1995; 39(3): 277–289.
4. Chorin AJ. Numerical Study of Slightly Viscous Flow. J. Fluid Mech. 1973; 136: 321–374.
5. Chorin AJ. Vortex Sheet Approximation of Boundary Layers. J. Comp. Phys. 1978; 27: 428–442.
6. Ghoniem AF, Chorin AJ, Oppenheim AK. Numerical Modelling of Turbulent Flow in a Combustion Tunnel. Phil. Trans. R. Soc. Lond. A. 1982; 304: 303–325.
7. White FM. Fluid Mechanics, 3rd Ed. New York: McGraw-Hill, Inc, 1994.
8. Lu QQ, Fontaine JR, Aubertin G. Particle Motion in Two-Dimensional Confined Turbulent Flows. Aerosol Science and Technology 1992; 17: 169–185.